1993

A Water and Heat Management Model for Proton-Exchange-Membrane Fuel Cells

Trung V. Nguyen
University of South Carolina - Columbia

Ralph E. White
University of South Carolina - Columbia, white@cec.sc.edu

Publication Info

Journal of the Electrochemical Society, 1993, pages 2178-2186.

Publisher's link: http://dx.doi.org/10.1149/1.2220792
DOI: 10.1149/1.2220792

A Water and Heat Management Model for Proton-Exchange-Membrane Fuel Cells

Trung V. Nguyen*,[a] and Ralph E. White*

Department of Chemical Engineering, University of South Carolina, Columbia South Carolina 29208

ABSTRACT

Proper water and heat management are essential for obtaining high-power-density performance at high energy efficiency for proton-exchange-membrane fuel cells. A water and heat management model was developed and used to investigate the effectiveness of various humidification designs. The model accounts for water transport across the membrane by electro-osmosis and diffusion, heat transfer from the solid phase to the gas phase and latent heat associated with water evaporation and condensation in the flow channels. Results from the model showed that at high current densities (> 1 A/cm^2) ohmic loss in the membrane accounts for a large fraction of the voltage loss in the cell and back diffusion of water from the cathode side of the membrane is insufficient to keep the membrane hydrated (*i.e.*, conductive). Consequently, to minimize this ohmic loss the anode stream must be humidified, and when air is used instead of pure oxygen the cathode stream must also be humidified.

Of various existing fuel cell systems, the proton-exchange-membrane (PEM) fuel cell is most promising, especially for terrestrial applications such as local power generation and transportation, because of the simplicity of its design and low temperature operations. The attractiveness of this fuel cell system has increased significantly within the past five years because of the following improvements. The catalyst loading has decreased from as high as 10 mg Pt/cm^2 to less than 0.5 mg Pt/cm^2.[1,3] Membranes with improved conductivity, water permeability, and thermal stability, such as the new perfluorosulfonic acid membrane from the Dow Chemical Company, have been developed.[4] Work to reduce the cost of material processing and preparation is also underway. The only remaining limiting design feature to the commercialization of this system is its ability to be operated at high power density and energy efficiency. (High power density translates to fewer cells required per unit power and hence lower system cost.)

Currently, to achieve high energy efficiency most PEM fuel cells operate at low current densities (consequently, lower power densities), and when high power density performance is obtained, it is achieved at the sacrifice of energy efficiency. Recent work has shown that proper water and heat management is one of the keys for achieving high power density performance at high energy efficiency. Proper heat removal and humidification are needed to keep the membrane well hydrated and conductive, which translates into lower ohmic losses and higher cell voltages.[5,6] Power densities greater than 1 W/cm^2 have been reported.[6-8]

In a proton exchange membrane fuel cell, the membrane acts both as a separator and as an electrolyte, see Fig. 1. The conductivity of this membrane is highly dependent on its hydration state.[9,10] During operation, due to the effect of electro-osmosis water molecules move from the anode to the cathode resulting in membrane dehydration on the anode side of the membrane[11] and flooding on the cathode side (additional water is produced at the cathode by the $O_2 + 4H^+ + 4e^- \rightarrow 2H_2O$ reaction). Previous results showed that water replenishment by back diffusion alone is insufficient to keep the anode side of the membrane hydrated especially at high current densities.[6,10-13] Furthermore, as the membrane becomes dehydrated the pores within the membrane shrink, resulting in lower water back-diffusion rates.[6,10,14,15] Any improper thermal management occurring during operation would exacerbate the water management problem.

The transport of water and ions in a proton exchange membrane fuel cell has been modeled at various levels of complexity by many groups. Verbrugge and Hill have developed various half-cell and full-cell models[16-18] to study the transport properties of perfluorosulfonic acid membranes under electrolyte supported condition (*i.e.*, the membrane was saturated with an electrolyte, typically sulfuric acid). Fales *et al.*[19] presented a model in which water transport by hydraulic permeation and electro-osmosis was assumed. The model was used to study the distribution of water within the membrane during operation. Fuller and Newman[20] developed a model which was based on concentrated solution theory to describe water transport in fuel cell membranes. Bernardi and Verbrugge[21-23] developed various models to study the effects of the transport of gases and water vapor in gas-diffusion electrodes on the performance of PEM fuel cells. In these models the membrane was assumed to be uniformly hydrated with constant transport properties, a case which may exist at low current densities and with "ultrathin" membranes. Recently, a more rigorous, isothermal model of a proton exchange membrane fuel cell was presented by Springer *et al.*[10] The model accounts for the dependence of the electro-osmotic coefficient on the water content within the membrane, gas transport within the diffusion layer of the electrodes, and water transport across the membrane by electro-osmotic force and back diffusion.

In general, all these models focused on the one-dimensional transport of the reactants and products in the electrodes and across the membrane. The model presented by Springer *et al.*[10] may be considered as a pseudo, one-step, two-dimensional model in which the flow channels were treated as being perfectly well mixed. The effects of the depletion of the reactants and the production of water at the cathode along the length of the fuel cell, and the combined effect of latent heat from water evaporation and condensation were not accounted for. Furthermore, all these models are isothermal and are unsuitable for water and heat management studies. Nguyen *et al.*[6] presented a two-dimensional heat and mass-transfer model for a PEM fuel cell, in which the electro-osmotic coefficient was assumed

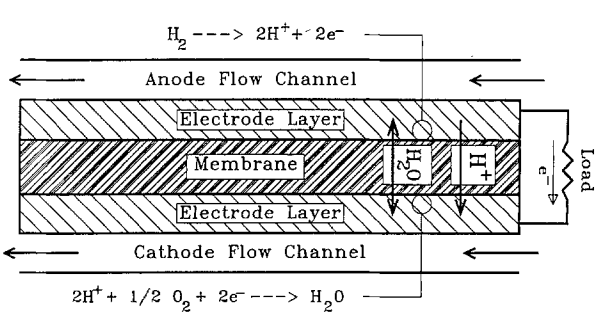

Fig. 1. Schematic of a proton-exchange-membrane (PEM) fuel cell.

* Electrochemical Society Active Member.
[a] Present address: AT&T Bell Laboratories, Mesquite, Texas 75149.

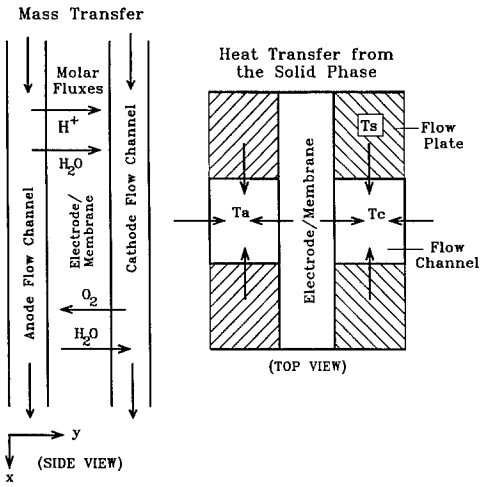

Fig. 2. Schematic of modeled regions.

to be constant. That model was devleoped as an exploratory design tool in the development of humidification systems for a PEM fuel cell. The model presented here was developed based on the experience gained from the model presented earlier by Nguyen *et al.*[6] and membrane transport data that have recently become available in the literature.

Model Description

This model is a steady-state, two-dimensional heat and mass-transfer model of a PEM fuel cell. The model regions consist of two flow channels on both sides of the membrane, one for the anode and the other for the cathode (refer to Fig. 2). The model accounts for mass transport of water and gaseous reactants across the membrane and along the flow channels and heat transport from the solid phases to the gases and *vice versa* along the flow channels. The assumptions used in the model are:

Assumptions.—

1. Because of the high thermal conductivities of the solid materials, the temperature of the solid (anode plates, electrodes, and membranes) is assumed to be uniform and constant.
2. Flow condition within the channel is plug-flow.
3. The total pressure is constant (that is, there is no pressure drop along the channels).
4. Heat transfer by conduction in the gas phase is negligible.
5. Water leaves the channels and enters the electrode/membrane in the form of vapor only.
6. Assuming that the electrode layer is "ultrathin," gas-diffusion through the electrode porous layer is neglected.
7. An ideal gas mixture is assumed.
8. Liquid water is assumed to exist in the form of small droplets and its volume is assumed to be negligible.
9. Since the anode side of the membrane is most likely to be drier than the cathode side due to the net water transport from the anode to the cathode at high current densities, the electro-osmotic coefficient and the diffusion coefficient of water in the membrane are assumed to be determined by the activity of the water in the anode flow channel.
10. Because of the high electronic conductivity of the current collectors, no voltage drop along the flow channels is assumed.

Material balance.—The change in the number of moles of a single-phase species i along the channel length is due to the normal flux in the y-direction into or out of the membrane.

$i = (H_2, O_2, N_2)$

$$\frac{dM_i}{dx} = -hN_{i,y,k}(x) \qquad [1]$$

Note that $N_{i,y,k}(x)$ is a function of x. It varies along the channel length because the current density changes along this direction as shown later. For water, the change in the number of moles due to condensation and evaporation are also included as shown in Eq. 2 and 3 below

Water, liquid

$$\frac{dM^l_{w,k}}{dx} = \left(\frac{k_c hd}{R(T_k + 273)}\right)\left(\frac{M^v_{w,k}}{M^v_{w,k} + M_{H_2/O_2}} P - P^{sat}_{w,k}\right) \qquad [2]$$

Water, vapor

$$\frac{dM^v_{w,k}}{dx} = -\frac{dM^l_{w,k}}{dx} - hN^v_{w,y,k}(x) \qquad [3]$$

where k_c is the homogeneous rate constant for the condensation and evaporation of water reaction; h and d are the width and height of the channel, respectively; and subscript k represents either the anode or cathode. The material balance on the liquid water depends on the difference between the partial pressure and the vapor pressure of water. That is, if the partial pressure of the water vapor is greater than the vapor pressure of water, water vapor will condense. Similarly, if the partial pressure of the water vapor is less than the vapor pressure and if there is any liquid water present, liquid water will evaporate to generate water vapor. Consequently, the change in the water vapor along the flow channels depends on both the change in the liquid water and the flux of water vapor in and out of the membrane, $N^v_{w,y,k}(x)$. The molar flux, $N_{i,y,k}$, for each component is

$$N_{H_2,y,a}(x) = \frac{I(x)}{2F} \quad N_{O_2,y,c(x)} = \frac{I(x)}{4F} \quad N_{N_2,y,c}(x) = 0 \qquad [4a]$$

and

$$N^v_{w,y,a}(x) = \frac{\alpha I(x)}{F} \quad N^v_{w,y,c}(x) = \frac{(1+2\alpha)I(x)}{2F} \qquad [4b]$$

where $I(x)$, the local current density of the fuel cell, varies along the channel length as the membrane conductivity and the electrodes overpotential change. F is the Faraday constant.

The parameter α represents the net water molecule per proton flux ratio and is calculated as follows

$$\text{New water flux} \equiv N^v_{w,y,a}(x) = \alpha \frac{I(x)}{F} = n_d \frac{I(x)}{F} - D_w \frac{dc_w}{dy} \qquad [5]$$

where the two terms on the right side of the equation represent the effects of migration and diffusion, respectively. This equation can be rearranged to obtain an expression for α

$$\alpha = n_d - \frac{F}{I(x)} D_w \frac{dc_w}{dy} \qquad [6]$$

To minimize the complexity of this model, we assume that the gradient of water concentration across the membrane can be approximated by a single-step linear difference between the concentration at the cathode and anode ($c_{w,c}$ and $c_{w,a}$), the final expression for α becomes

$$\alpha = n_d - \frac{F}{I(x)} D_w \frac{(c_{w,c} - c_{w,a})}{t_m} \qquad [7]$$

where n_d, D_w, and t_m are the electro-osmotic coefficient (= number of water molecules carried by a proton), diffusion coefficient of water in the membrane, and membrane thickness, respectively. This electro-osmotic coefficient depends on the water content in the membrane, which in turn depends on the activity of water in the gas phase next to the membrane.[10]

At high current densities, the water transport rate by electro-omosis from the anode to cathode exceeds the back diffusion rate of water from the cathode to the anode. This results in a net water transport rate from the anode to the cathode, and as a result, partial dehydration along the anode and saturation along the cathode.[11] Based on this observation, it is reasonable to assume that the water content

in the membrane is most likely lower on the anode side, and consequently the activity of the water on the anode side can be used to calculate the electro-osmotic coefficient across the whole membrane (Assumption No. 9). We could use the average of the activity of water in the anode and cathode as another approach. However, we chose to use this more conservative approach. Expressions given by Springer *et al.*[10] are used to calculate the following equation for n_d as a function of the activity of water in the anode flow channel, a_a

$$n_d = 0.0049 + 2.02a_a - 4.53a_a^2 + 4.09a_a^3 \quad (\text{for } a_a \le 1) \quad [8a]$$

and

$$n_d = 1.59 + 0.159(a_a - 1) \quad (\text{for } a_a > 1) \quad [8b]$$

Based on the same assumption, the diffusion coefficient of water is given by the following expression

$$D_w = (0.0049 + 2.02a_a - 4.53a_a^2 + 4.09a_a^3)D^\circ \exp\left[2416\left(\frac{1}{303} - \frac{1}{273 + T_s}\right)\right] \quad (\text{for } a_a \le 1) \quad [9a]$$

and

$$D_w = [1.59 + 0.159(a_a - 1)]D^\circ \exp\left[2416\left(\frac{1}{303} - \frac{1}{273 + T_s}\right)\right] \quad (\text{for } a_a > 1) \quad [9b]$$

The expression for the diffusion coefficient of water in the membrane given by Springer *et al.* was found to be inappropriate because the values obtained turned out to be almost independent of the water content in the membrane. When this expression was used, the model predicted that the fuel cell could operate at high current densities (> 1 A/cm^2) without humidification for the anode gas stream. Since our data and those available in the literature for fuel cells using Nafion[R,6,11] do not support this observation, we decided to use a different expression. Due to the lack of data, an assumption was made here that the diffusion coefficient of water in the membrane would be dependent on the water content in the membrane in a similar manner as the electro-osmotic coefficient. This expression can be modified when additional data or new expression for the diffusion coefficient of water in the membrane becomes available.

Finally, the expressions for $c_{w,c}$ and $c_{w,a}$ are given below[10]

$$c_{w,k} = \frac{\rho_{m,dry}}{M_{m,dry}}(0.043 + 17.8a_k - 39.8a_k^2 + 36.0a_k^3) \quad \text{for } a_k \le 1 \quad [10]$$

$$c_{w,k} = \frac{\rho_{m,dry}}{M_{m,dry}}[14 + 1.4(a_k - 1)] \quad \text{for } a_k > 1 \quad [11]$$

where the subscript k represents either the anode or cathode, and $\rho_{m,dry}$ and $M_{m,dry}$ are the density and the equivalent weight of a dry proton exchange membrane. The activities of water in the anode and cathode streams are defined as follows

Anode

$$a_a = \frac{x_{w,a}P}{P_{w,a}^{sat}} = \left(\frac{\dot{M}_{w,a}^v}{\dot{M}_{w,a}^v + \dot{M}_{H_2}}\right)\frac{P}{P_{w,a}^{sat}} \quad [12]$$

Cathode

$$a_c = \frac{x_{w,c}P}{P_{w,c}^{sat}} = \left(\frac{\dot{M}_{w,c}^v}{\dot{M}_{w,c}^v + \dot{M}_{O_2} + \dot{M}_{N_2}}\right)\frac{P}{P_{w,c}^{sat}} \quad [13]$$

The expression for the vapor pressure for water as a function of temperature is[10]

$$\log_{10}(P_{w,k}^{sat}) = 2.95 \cdot 10^{-2}T_k - 9.18 \cdot 10^{-5}T_k^2 + 1.44 \cdot 10^{-7}T_k^3 - 2.18 \quad [14]$$

where the subscript k represents either the anode or the cathode.

Energy balance.—The energy balance equation for the anode and cathode gaseous streams is

$$\sum_i (\dot{M}_i C_{p,i})\frac{dT_k}{dx} = (H_{w,k}^v - H_{w,k}^l)\frac{d\dot{M}_{w,k}^l}{dx} + Ua(T_s - T_k) \quad [15]$$

where the subscript k represents either the anode or the cathode. The parameter U is the overall heat-transfer coefficient, and the parameter a is the heat-transfer area per unit length of the flow channel [$=2(h + d)$]. The first term on the left side of Eq. 8 accounts for the enthalpy change due to condensation or evaporation of water in the flow channel. Values for the heat of evaporation or condensation, $(H_{w,k}^v - H_{w,k}^l)$ as a function of temperature can be calculated from the following equation[24]

$$(H_{w,k}^v - H_{w,k}^l) = 45{,}070 - 41.9T + 3.44 \cdot 10^{-3}T^2 + 2.54 \cdot 10^{-6}T^3 - 8.98 \cdot 10^{-10}T^4 \quad [16]$$

Cell potential.—The cell potential can be calculated from the membrane resistance and electrode polarizations as follows

$$V_{cell} = V_{oc} - \eta(x) - \frac{I(x)t_m}{\sigma_m(x)} \quad [17]$$

where V_{oc} is the open-circuit potential of the fuel cell and $\eta(x)$ is the cell overpotential. By assuming that the cell overpotential is located mainly in the cathode, $\eta(x)$ can be calculated from the following equation[10]

$$\eta(x) = \frac{R(273 + T_s)}{0.5F}\ln\left(\frac{I(x)}{I^\circ P_{O_2}(x)}\right) \quad [18]$$

where I° is the exchange current density at one atmosphere of oyxgen, and $P_{O_2}(x)$ is the partial pressure of oxygen in the cathode stream, respectively. Since the solid-phase temperature, which is also the fuel cell temperature, is assumed to be constant with time and distance, the dependence of the exchange current density and the open-circuit potential on temperature is neglected. Different values will be used for different fuel cell operating temperatures. The membrane conductivity, $\sigma_m(x)$, calculated as a function of the water content in the membrane at the anode interface is[10]

$$\sigma_m(x) = \left(0.00514\frac{M_{m,dry}}{\rho_{m,dry}}c_m(x) - 0.00326\right) \cdot \exp\left(1268\left[\frac{1}{303} - \frac{1}{273 + T_s}\right]\right) \quad [19]$$

The final equations used in the model are given in Table I along with the equations for the heat capacities, $C_{p,i}$, of each component obtained from Ref. 24. There are nine governing equations for the nine unknowns, $\dot{M}_{H_2}$, $\dot{M}_{O_2}$, $\dot{M}_{N_2}$, $\dot{M}_{w,a}^v$, $\dot{M}_{w,a}^l$, $\dot{M}_{w,c}^v$, $\dot{M}_{w,c}^l$, T_a, and T_c, and 27 supporting equations for the parameters used in the governing equations.

Solution technique.—The model is solved as follows. An average current density, I_{avg}, is specified where

$$I_{avg} = \frac{1}{L}\int_0^L I(x)dx \quad [20]$$

The parameter L is the channel length and $I(x)$ is the local current density at every point along the channel length. Based on the value of I_{avg}, flow rates for hydrogen, oxygen, nitrogen (if air is used), and water vapor and liquid are calculated. Next, a guessed value for the cell voltage is chosen and the model equations are solved to get a set of $I(x)$ and I_{avg} from Eq. 20. If the calculated I_{avg} is not equal to the specified I_{avg}, a different cell voltage is chosen. This process is repeated until the calculated I_{avg} agrees with the specified I_{avg} to within three digits. Instead of iterating the model manually, an iteration loop based on the Newton-Raphson method is used to help search for the correct cell voltage

$$V^{n+1}_{guess} = V^{n}_{guess} - \frac{F(V^{n}_{guess})}{F'(V^{n}_{guess})} \quad [21]$$

where

$$F(V^{n}_{guess}) = I^{calc}_{avg}(V^{n}_{guess}) - I^{spec}_{avg} \quad [22]$$

and $F'(V^{n}_{guess})$ is calculated numerically as follows

$$F'(V^{n}_{guess}) = \frac{F([1+\delta]\cdot V^{n}_{guess}) - F(V^{n}_{guess})}{\delta \cdot V^{n}_{guess}} \quad [23]$$

A perturbation (δ) of 0.001 is used.

Within the model, fourth-order Runge-Kutta method is used to solve along the flow channel direction. Proper step size is chosen to obtain at least five-digit accuracy. Within each Runge-Kutta step, another iteration loop based on the Newton-Raphson method is used to search for the correct local current density, $I(x)$, that will yield the guessed cell voltage

$$I(x)^{j+1} = I(x)^{j} - \frac{F[I(x)^{j}]}{F'[I(x)^{j}]} \quad [24]$$

where

$$F[I(x)^{j}] = V^{j}_{cal}(x) - V_{guess} \quad [25]$$

and

$$F'[I(x)^{j}] = \frac{F[(1+\delta)\cdot I(x)^{j}] - F[I(x)^{j}]}{\delta \cdot I(x)^{j}} \quad [26]$$

$F'[I(x)^{j}]$ is also calculated numerically with a perturbation (δ) of 0.001. To obtain a voltage-current curve, cell voltages are calculated for a range of I_{avg}. Table II shows values for

Table I. Governing equations for the water and heat management model.

Anode

Hydrogen:
$$\dot{M}_{H_2} = \dot{M}^{o}_{H_2} - \frac{hI(x)}{2F}x \quad [I\text{-}1]$$

Water, liquid:
$$\frac{d\dot{M}^{l}_{w,a}}{dx} = \left(\frac{hd}{R(T_a+273)}\right)\left(\frac{\dot{M}^{v}_{w,a}}{\dot{M}^{v}_{w,a}+\dot{M}_{H_2}}P - P^{sat}_{w,a}\right) \quad [I\text{-}2]$$

Water, vapor:
$$\frac{d\dot{M}^{v}_{w,a}}{dx} = -\frac{d\dot{M}^{l}_{w,a}}{dx} - \frac{\alpha I(x)h}{F} \quad [I\text{-}3]$$

T(a):
$$\sum_i (\dot{M}_i C_{p,i})\frac{dT_a}{dx} = (H^{v}_{w,a} - H^{l}_{w,a})\frac{d\dot{M}^{l}_{w,a}}{dx} + Ua(T_s - T_a) \quad [I\text{-}4]$$

Cathode

Oxygen:
$$\dot{M}_{O_2} = \dot{M}^{o}_{O_2} - \frac{hI(x)}{4F}x \quad [I\text{-}5]$$

Nitrogen:
$$\dot{M}_{N_2} = \dot{M}^{o}_{N_2} \quad [I\text{-}6]$$

Water, liquid:
$$\frac{d\dot{M}^{l}_{w,c}}{dx} = \left(\frac{hd}{R(T_c+273)}\right)\left(\frac{\dot{M}^{v}_{w,c}}{\dot{M}^{v}_{w,c}+\dot{M}_{O_2}+\dot{M}_{N_2}}P - P^{sat}_{w,c}\right) \quad [I\text{-}7]$$

Water, vapor:
$$\frac{d\dot{M}^{v}_{w,a}}{dx} = -\frac{d\dot{M}^{l}_{w,a}}{dx} - \frac{I(x)h(1+2\alpha)}{2F} \quad [I\text{-}8]$$

T(c):
$$\sum_i (\dot{M}_i C_{p,i})\frac{dT_c}{dx} = (H^{v}_{w,c} - H^{l}_{w,c})\frac{d\dot{M}^{l}_{w,c}}{dx} + Ua(T_s - T_c) \quad [I\text{-}9]$$

$$\alpha = n_d - \frac{F}{I(x)}D_w\frac{(c_{w,c} - c_{w,a})}{t_m} \quad [I\text{-}10]$$

$$n_d = 0.0049 + 2.024a_a - 4.53a_a^2 + 4.09a_a^3 \quad (\text{for } a_a \le 1) \quad [I\text{-}11]$$

$$n_d = 1.59 + 0.159(a_a - 1) \quad (\text{for } a_a > 1) \quad [I\text{-}12]$$

$$D_w = (0.0049 + 2.02a_a - 4.53a_a^2 + 4.09a_a^3)D^\circ \exp\left[2416\left[\frac{1}{303} - \frac{1}{273+T_s}\right]\right] \quad (\text{for } a_a \le 1) \quad [I\text{-}13a]$$

$$D_w = [1.59 + 0.159(a_a - 1)]D^\circ \exp\left[2416\left[\frac{1}{303} - \frac{1}{273+T_s}\right]\right] \quad (\text{for } a_a > 1) \quad [I\text{-}13b]$$

$$c_{w,k} = \frac{\rho_{m,dry}}{M_{m,dry}}(0.043 + 17.8a_k - 39.85a_k^2 + 36.0a_k^3) \quad \text{for } a_k \le 1 \quad [I\text{-}14]$$

$$c_{w,k} = \frac{\rho_{m,dry}}{M_{m,dry}}[14 + 1.4(a_k - 1)] \quad \text{for } a_k > 1 \quad [I\text{-}15]$$

$$a_a = \frac{x_{w,a}P}{P^{sat}_{w,a}} = \left(\frac{\dot{M}^{v}_{w,a}}{\dot{M}^{v}_{w,a}+\dot{M}_{H_2}}\right)\frac{P}{P^{sat}_{w,a}} \quad [I\text{-}16]$$

$$a_c = \frac{x_{w,c}P}{P^{sat}_{w,c}} = \left(\frac{\dot{M}^{v}_{w,c}}{\dot{M}^{v}_{w,c}+\dot{M}_{O_2}+\dot{M}_{N_2}}\right)\frac{P}{P^{sat}_{w,c}} \quad [I\text{-}17]$$

$$\log_{10}(P^{sat}_{w}) = 2.95\cdot 10^{-2}T_k - 9.18\cdot 10^{-5}T_k^2 + 1.44\cdot 10^{-7}T_k^3 - 2.18 \quad [I\text{-}18]$$

$$(H^{v}_{w,k} - H^{l}_{w,k}) = 45{,}070 - 41.94T_k + 3.44\cdot 10^{-3}T_k^2 + 2.54\cdot 10^{-6}T_k^3 - 8.98\cdot 10^{-10}T_k^4 \quad [I\text{-}19]$$

$$C^{l}_{p,w} = 75.38 \text{ J/mol/°C} \quad [I\text{-}20]$$

$$C^{v}_{p,w} = 33.46 + 6.88\cdot 10^{-3}T_k + 7.60\cdot 10^{-6}T_k^2 - 3.59\cdot 10^{-9}T_k^3 \text{ J/mol/°C} \quad [I\text{-}21]$$

$$C_{p,H_2} = 28.84 + 7.65\cdot 10^{-5}T_k + 3.29\cdot 10^{-6}T_k^2 - 8.70\cdot 10^{-10}T_k^3 \text{ J/mol/°C} \quad [I\text{-}22]$$

$$C_{p,O_2} = 29.10 + 1.16\cdot 10^{-3}T_k - 6.08\cdot 10^{-6}T_k^2 + 1.31\cdot 10^{-9}T_k^3 \text{ J/mol/°C} \quad [I\text{-}23]$$

$$C_{p,N_2} = 29.00 + 2.20\cdot 10^{-3}T_k + 5.72\cdot 10^{-6}T_k^2 - 2.87\cdot 10^{-9}T_k^3 \text{ J/mol/°C} \quad [I\text{-}24]$$

$$V_{cell} = V_{oc} - \eta(x) - \frac{I(x)t_m}{\sigma_m(x)} \quad [I\text{-}25]$$

$$\eta(x) = \frac{R(273+T_s)}{0.5F}\ln\left(\frac{I(x)}{I^\circ P_{O_2}(x)}\right) \quad [I\text{-}26]$$

$$\sigma_m(x) = (0.00514\frac{M_{m,dry}}{\rho_{m,dry}}c_m(x) - 0.00326)\cdot \exp\left(1268\left[\frac{1}{303} - \frac{1}{273+T_s}\right]\right) \quad [I\text{-}27]$$

Table II. Values for parameters used in the base case.

Channel width (h)	0.2 cm
Channel height (d)	0.2 cm
Channel length (L)	10 cm
Current density (I_{avg})	1 A/cm^2
Total pressure (P)	2 atm. absolute
Heat-transfer coefficient (U)	0.0025 J/s/cm^2/°C
Condensation rate constant (k_c)	1.0 s^{-1}
Temperature of solid phase (T_s)	90°C
Membrane dry density ($\rho_{m,dry}$)	2.0 g/cm^3
Membrane dry equivalent weight ($M_{m,dry}$)	1100
Membrane thickness (t_m)	0.01275 cm
Fuel cell open-circuit voltage (V_{oc})	1.1 V
Oxygen exchange current density (I°)	0.01 A/cm^2
D°	5.5 × 10^{-7} cm^2/s
Anode:	
Inlet temperature (T_a)	90°C
Hydrogen flow rate ($\dot{M}^{\circ}_{H_2}$)	1.5 × I_{avg}
Inlet water, vapor ($\dot{M}^{vo}_{w,a}$)	Saturated
Inlet water, liquid ($\dot{M}^{lo}_{w,a}$)	0 × $\dot{M}^{\circ}_{H_2}$
Cathode:	
Inlet temperature (T_c)	90°C
Oxygen flow rate ($\dot{M}^{\circ}_{O_2}$)	2.0 × I_{avg}
Nitrogen flow rate ($\dot{M}^{\circ}_{N_2}$)	0
Inlet water, vapor ($\dot{M}^{vo}_{w,c}$)	Dry
Inlet water, liquid ($\dot{M}^{lo}_{w,c}$)	0 × ($\dot{M}^{\circ}_{O_2}$ + $\dot{M}^{\circ}_{N_2}$)

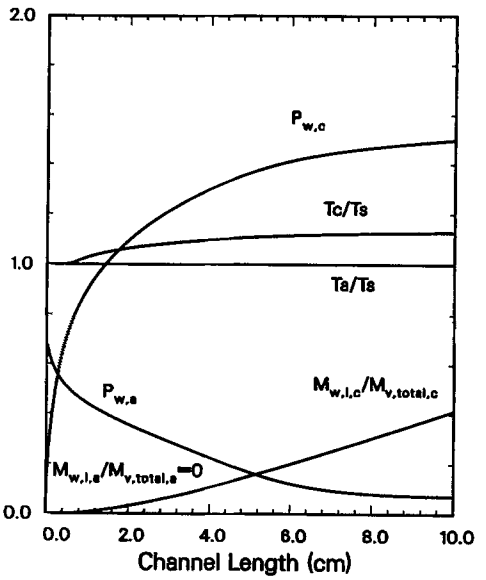

Fig. 4. Water and temperature profiles along the flow channels for the base case.

the input parameters for the base case. Other case studies are variations of the base case.

Results and Discussion

As stated earlier, during the operation water molecules are carried from the anode side to the cathode side of the membrane by electro-osmosis, and if this transport rate of water is higher than that by back-diffusion of water the membrane will eventually become dehydrated and too resistive to conduct high current. Consequently, to prevent membrane dehydration a sufficient amount of water must be added to the anode stream to make up for the amount of water lost due to the net transport of water from the anode to the cathode. Figure 3 shows four humidification designs that can be used for PEM fuel cells.[12]

In the conventional design, the incoming gas stream is saturated with water prior to entering the fuel cell. Humidification temperature 10 to 15°C higher than the fuel cell temperature is often used to increase the amount of water introduced into the cell. In the "vapor injection" design, water vapor is introduced into the electrode chamber at various points along the flow channel to make up for the amount consumed by the net water flux from the anode to the cathode. There are various ways that water can be added in the vapor injection design. One way is to use a porous backing plate for flow channels with water on one side of the plate and the anode stream on the other.[11] This allows water to be continuously added to the gas stream over the whole length of the flow channels. In the third design, the gas stream is quickly recirculated through an external humidifier to keep the gas stream continuously

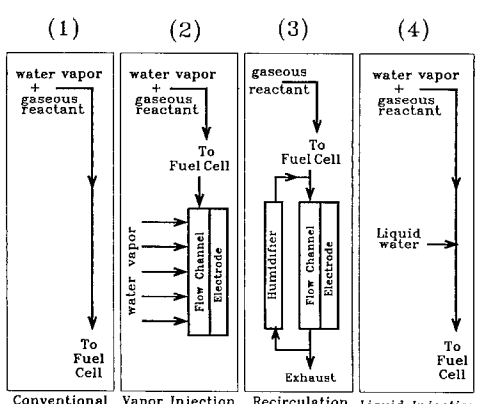

Fig. 3. Humidification designs for PEM fuel cells.

saturated. These two approaches have been tested and found to work.[6,11] However, they require complex electrode designs and flow controls.

The fourth design is a modification of the conventional design in which an additional amount of liquid water is injected directly into the fuel cell. This "liquid injection" design was based on the concept that as water vapor in the gas stream is lost to the membrane due to the electro-osmotic effect, additional water in liquid form will evaporate to make up for this loss. Furthermore, the heat removal characteristic of this "evaporative cooling" process can be used for thermal management. The model developed here will be used to evaluate (*i*) the "liquid injection" design in comparison to the conventional design and (*ii*) the humidification problems associated with air operation.

A base case which corresponds to a PEM fuel cell operating with pure hydrogen and oxygen at 2 atm absolute, 90°C, and a current density of 1 A/cm^2 is evaluated first. The inlet streams are saturated with water using the conventional humidification design. The humidification temperature is chosen to be the same as the cell temperature. The physical and transport values used (Eq. 8-11) represent those of a Nafion^R, 1100 equivalent weight.[10] Fuel cell performance with the Dow's experimental membranes will be investigated when the transport properties of these membranes become available. Other parameters for the base case are given in Table II. In the development of the equation for the homogeneous condensation and evaporation reaction expression, Eq. 2, it was assumed that the reaction is complete and instantaneous. Rate constants equal to or greater than 1 s^{-1} were found to satisfy this assumption. The value of 1 s^{-1} was used here because values equal to or greater than 10 s^{-1} were found to result in instability and convergence problems. Finally, for the overall heat-transfer coefficient used in Eq. 15, a value of 0.0025 J/s-cm^2-°C was used as compared to the value of 0.0036 J/s-cm^2-°C that was used by Fuller and Newman in Ref. 5. We based our value on half the value given for the iron/water vapor system.[25]

Base case.—The results for the base case are shown in Fig. 4-8. Except for the partial pressures of water vapor, all parameters in Fig. 4 are plotted in dimensionless forms. Masses of liquid water are divided by the total initial masses of the gases; and temperatures are divided by the solid-phase temperature. Figure 4 shows that the amount of water vapor ($P_{w,a}$) in the anode stream decreases quickly within the first half of the flow channel length and levels off to a small value. This observation can be explained as follows. Near the inlet of the fuel cell where the membrane is well hydrated and highly con-

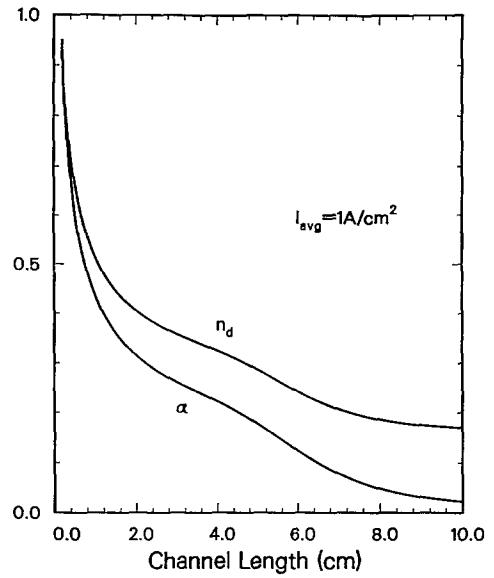

Fig. 5. A comparison of the net water transport per proton and the electro-osmotic coefficient along the flow channels for the base case.

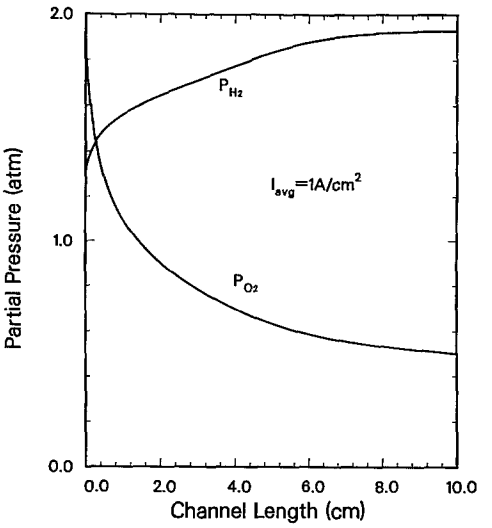

Fig. 7. Partial pressures of oxygen and hydrogen along the flow channels for the base case.

ductive, the electro-osmotic drag coefficient is higher (see curve for n_d in Fig. 5) and the current carrying capability of the membrane is higher (see current distribution curve in Fig. 8). Furthermore, since the cathode gas stream enters the fuel cell dry, the water content in the cathode stream is low and therefore the amount of water transported back to the anode by back diffusion is low. All these processes translate to high net flux of water across the membrane (see curve for α in Fig. 5), high current density, and high depletion rates of hydrogen and oxygen within this region (see Fig. 7).

Down the channel, the water content in the anode gas stream decreases which translates to a decrease in the water content in the membrane, electro-osmotic drag coefficient, and membrane conductivity. Additionally, with higher water content in the cathode side water transport from the cathode back to the anode by diffusion is greater. Consequently, the local current density decreases and the net water flux across the membrane also decreases, resulting in a lower depletion rate of water from the anode gas stream, a lower production rate of water in the cathode, and a lower depletion rate of hydrogen and oxygen.

Figure 4 also shows water condensation occurring in the cathode channel once the partial pressure of water in the cathode stream exceeds the water vapor pressure. The amount of liquid water increases as more water is generated from the oxygen reaction and transported from the anode. Note also the increase in the temperature of the cathode stream as a result of the latent heat from water condensation. The temperature of the anode gas stream does not change because the anode incoming gas entered at the cell temperature, and no phase changes occurred.

Finally, Fig. 6 shows that voltage loss in a PEM fuel cell due to the ionic resistance of the membrane is significant at high current density. For the base case (*i.e.*, at 1 A/cm^2) this voltage loss is twice the amount due to the overpotential of the cathode electrode. The general assumption that most of the potential loss in a PEM fuel cell is due to the overpotential in the oxygen cathode electrode does not apply at these current density and conditions.

Effect of using higher humidification temperatures.— One of the approaches often employed by fuel cell designers to overcome the water starvation problem is to raise the humidification temperature. This allows a larger amount of water to be carried into the anode. Problems such as thermal stress on the membrane and electrode flooding as a result of water condensation from the temperature difference between the hot, water-saturated incoming gas and the cooler fuel cell limit the humidification temperature to typically 10 to 15°C above the fuel cell temperature. The model is used here to evaluate the effect of using an anode

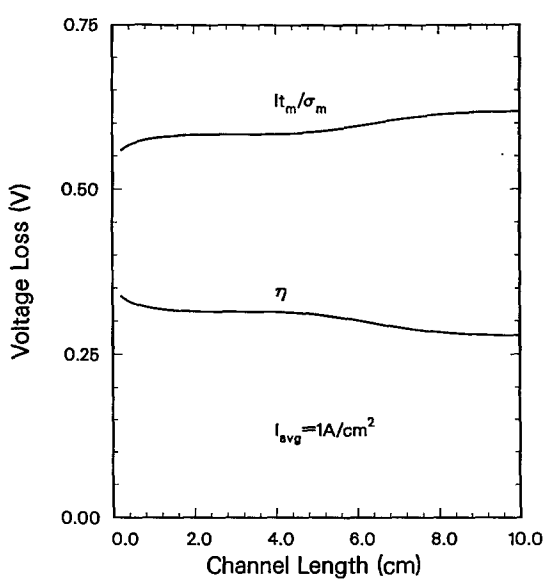

Fig. 6. Voltage loss due to the oxygen reaction and the ohmic resistance of the membrane for the base case.

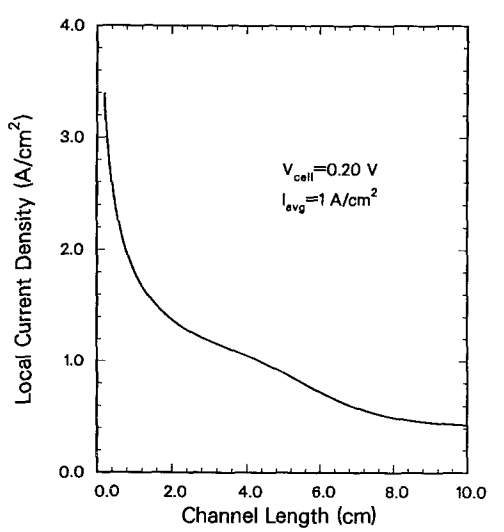

Fig. 8. Current distribution along the flow channels for the base case.

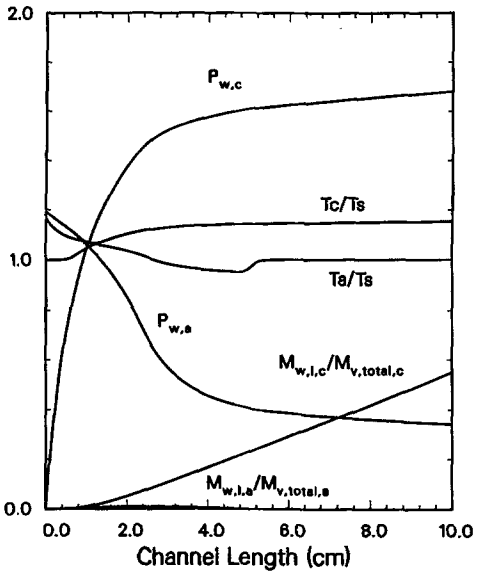

Fig. 9. Water and temperature profiles along the flow channels for the $T_{a,in}$ = 105°C case.

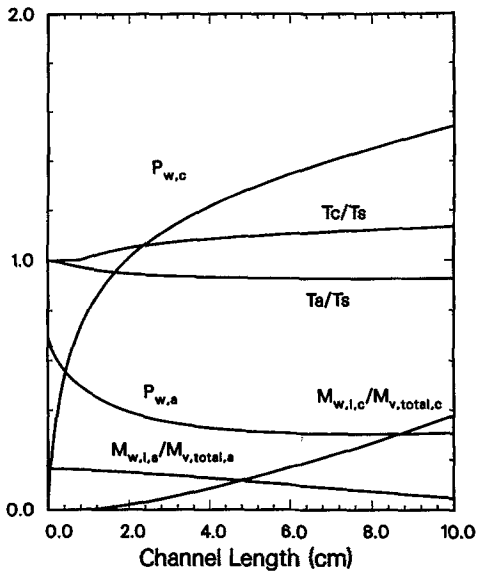

Fig. 10. Water and temperature profiles along the flow channels for the liquid injection and $T_{a,in}$ = 90°C case.

humidification temperature of 105°C. Other conditions are similar to the base case.

Figure 9 shows that by increasing the anode humidification temperature from 90 to 105°C the partial pressure of water increases from 0.7 to 1.2 atm, thus allowing more water to be introduced into the fuel cell. This extra amount of water helps keep the membrane better hydrated, resulting in higher ionic conductivity and higher cell voltage (0.58V *vs.* 0.20V) at the same average current density as the base case (1 A/cm^2). Note that the partial pressure of water at the outlet for this case is higher than that in the last 80% of the channel length of the base case. Other differences are temperature changes in the anode gas stream. As the hotter anode stream entering the cell cools as it comes in contact with cooler surfaces in the cell, a small amount of water condenses. This small amount of liquid water evaporates farther down the channel as the partial pressure of water decreases as a result of the net water transport across the membrane, causing further decrease in the gas temperature. Once the liquid water is completely consumed, the temperature of the anode gas stream increases as heat is transferred from the solid phase to the gas phase. The performance of a fuel cell with this humidification design at various current densities will be shown later in Fig. 12.

Effectiveness of the liquid injection design.—Next, the model is used to evaluate the effectiveness of the liquid injection humidification design. In this case, the anode stream enters the fuel cell saturated with water at the fuel cell temperature (90°C) and an additional amount of 90°C liquid water equivalent to 25% the amount of hydrogen in the feed stream is injected into the fuel cell. In practice, the liquid water is injected into the flowing gas stream as small atomized droplets.

Comparing the results given in Fig. 4 for the base case and those given in Fig. 10 for the liquid injection case shows similar trends except for two major differences. With this design, the partial pressure of water stops decreasing beyond four-tenths the length of the channel because there is sufficient liquid water in the system to evaporate and replenish the loss water vapor due to the net water transport across the membrane. However, the partial pressure of water in the cell and the cell voltage (0.48 V) are not as high as those of the higher humidification temperature case. This is due to the lower temperature of the anode stream in the liquid injection case which occurs as a result of the evaporation of liquid water and that the heat-transfer rate from the solid phase to the gas phase is not high enough to maintain a higher anode stream temperature. Better performance (higher voltage) might be possible with a higher heat-transfer rate between the solid phase and the gas phase. This could be achieved by increasing the heat-transfer surface area and using materials with higher heat-transfer coefficients.

Figure 11 shows the current distribution along the flow channels for the three different humidification cases. Note that the base case has the most nonuniform current distribution followed by the higher humidification temperature case and then by the liquid injection case. If thermal stress and stress due to nonuniform current distribution on the membrane are important, this aspect needs to be considered in the design of PEM fuel cells. Figure 12 shows the voltage-current curves for the three humidification cases investigated here. Note that at low current densities (< 0.3 A/cm^2) where the performance is kinetically controlled (that is, the overpotential of the oxygen electrode is much higher than the voltage loss due to the ionic resistance of the membrane) there are no differences between these humidification designs. However, at higher current densities where the effect of the membrane ionic resistance is significantly higher the advantages of having an optimal water management system becomes obvious, as shown by the higher voltages of the cases with better humidification.

Finally, the results shown in Fig. 13 further illustrated the need to have the anode stream humidified. In this fig-

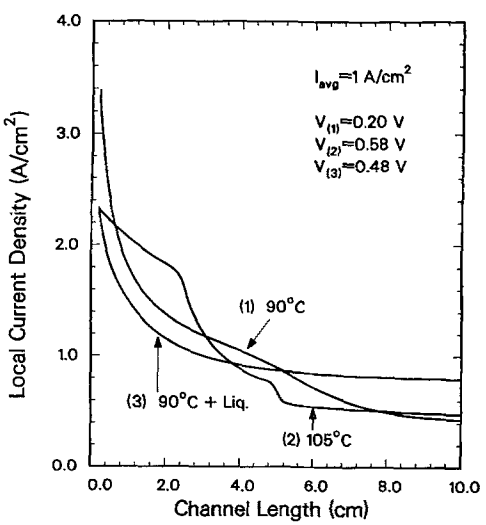

Fig. 11. Current distribution along the flow channels for three different humidification designs.

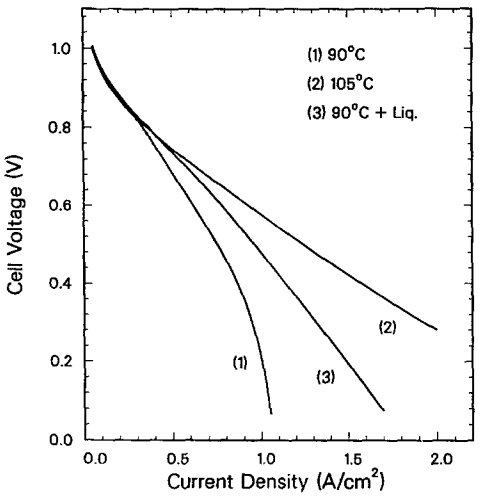

Fig. 12. The effect of humidification designs on the performance of a PEM fuel cell.

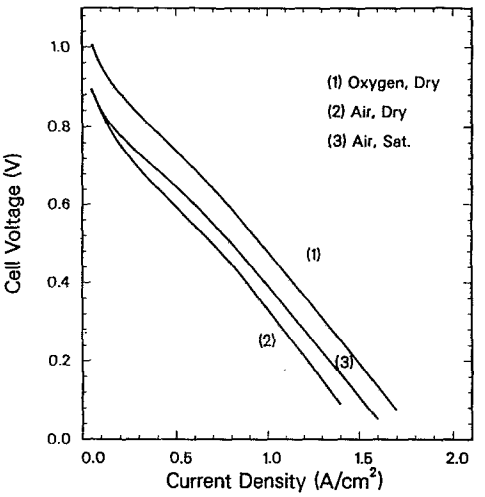

Fig. 14. The effect of using dry air and water-saturated air on the performance of a PEM fuel cell.

ure, α and n_d denote the net number of water molecules transported across the membrane per proton and the number of water molecules dragged across the membrane by electro-osmosis. Their values are averaged values over the whole channel length. Note that at low current densities the difference between α and n_d is larger because the back-diffusion rate of water from the cathode to the anode matches the electro-osmotic rate. However, at higher current densities the back-diffusion rate of water becomes insufficient and the net water transport rate across the membrane approaches that by electro-osmosis.

Effect of using air.—For applications such as in transportation in which the weight penalty of oxygen tanks is not acceptable, air is used. In this case the effect of using air instead of pure oxygen is evaluated, and the need to have the cathode (air) stream humidified is demonstrated. When humidified air is used, it is assumed to enter the cell saturated with water at the cell temperature. The anode gas stream is humidified by liquid injection similarly to the previous case. Other conditions are identical to the base case.

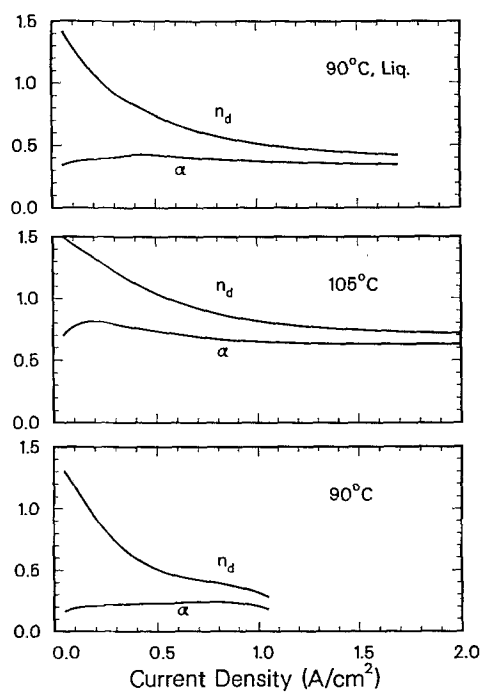

Fig. 13. Net water flux per proton and the electro-osmotic coefficient at various current densities for the three humidification designs.

The results shown in Fig. 14 illustrates that better performance will be obtained if the air stream is also humidified. This observation, which has been verified experimentally,[7,10] can be explained as follows. The poor performance of dry air operation is attributed to two factors: low oxygen partial pressure in air and higher membrane dehydration. When air is used, to get the same amount of oxygen a much larger gas flow rate is needed. This high flow rate of dry gas keeps the partial pressure of water on the cathode side of the membrane low. As a result, water transport by diffusion is now in the same direction as that of electro-osmosis: from the anode to the cathode. This combined affect increases the net transport rate of water across the membrane and results in a higher consumption rate of water from the anode stream and eventually membrane dehydration. Consequently, by humidifying the air stream back diffusion is promoted, resulting in lower net water transport across the membrane.

Finally, even though the effects of the fuel cell operating temperature were not investigated, it could be done by changing the values used for the solid phase, T_s.

Conclusions

A heat and water management model for proton-exchange-membrane fuel cells has been developed. The model was used to evaluate the effectiveness of three humidification strategies and the effect of air operation. The results show that back diffusion of water from the cathode to the anode is insufficient to keep the membrane hydrated at high power densities and energy efficiency operations. Consequently, the anode gas stream must be humidified. The results also show that when air is used the cathode stream must also be humidified. The model presented here can be used as a design tool to evaluate the effectiveness of various heat removal and humidification designs and the effects of various design and operating parameters on the performance of a PEM fuel cell. These results can then be used to help determine an optimal fuel cell design for a specific application.

Manuscript submitted Dec. 5, 1992; revised manuscript received April 2, 1993.

The University of South Carolina assisted in meeting the publication costs of this article.

LIST OF SYMBOLS

a	heat transfer area per unit length, cm
a_k	activity of water in stream k
d	channel height, cm
D°	a parameter used in the expression for diffusion coefficient of water, cm²/s
D_w	diffusion coefficient of water, cm²/s
$C_{p,i}$	heat capacity of gas i, J/mol/°C
$C_{p,w}^l$	heat capacity of liquid water, J/mol/°C
$C_{p,w}^v$	heat capacity of water vapor, J/mol/°C

c_w	concentration of water in the membrane, mol/cm^3
$c_{w,k}$	concentration of water at k interface of the membrane, mol/cm^3
F	Faraday constant, 96487 C/equivalent
h	channel width, cm
$H^v_{w,k}$	enthalpy of water vapor in k stream, J/mol
$H^l_{w,k}$	enthalpy of liquid water in k stream, J/mol
I	local current density, A/cm^2
I_{avg}	cell average current density, A/cm^2
I°	exchange current density for the oxygen reaction, A/cm^2
k_c	evaporation and condensation rate constant, s^{-1}
L	channel length, cm
M_i	molar flow rate of species i, mol/s
$M_{m,dry}$	equivalent weight of a dry membrane, g/mol
$\dot{M}^l_{w,k}$	molar flow rate of water vapor in k channel, mol/s
$\dot{M}^v_{w,k}$	molar flow rate of water vapor in k channel, mol/s
n_d	electro-osmotic drag coefficient (number of water molecules carried per proton)
$N_{i,y,k}$	y-component molar flux of species i in k channel, mol/s/cm^2
$N^v_{w,y,k}$	y-component molar flux of water vapor in k channel, mol/s/cm^2
P	cell total pressure, atm
P_i	partial pressure of species i, atm
$P^{sat}_{w,k}$	vapor pressure of water in k channel, atm
R	gas constant, 82.06 cm^3 atm/mol/K or 8.314 J/mol/K
t_m	membrane thickness, cm
T_a	temperature of the anode stream, °C
T_c	temperature of the cathode stream, °C
T_s	temperature of the solid phase, °C
U	overall heat-transfer coefficient, J/s/cm^2/°C
V_{oc}	cell open-circuit voltage, V
V_{cell}	cell voltage, V
x	direction along the channel length, cm
$x_{w,k}$	mole fraction of water in k stream
y	direction normal to the channel length, cm

Greek

α	net water flux per proton flux
η	overpotential for the oxygen reaction, V
$\rho_{m,dry}$	density of a dry membrane, g/cm^3
σ_m	membrane conductivity, 1/Ω/cm

Subscripts and superscripts

a	anode
c	cathode
H_2	hydrogen
k	anode or cathode
m	membrane
N_2	nitrogen
O_2	oxygen
w	water
y	y-direction
v	vapor
l	liquid
sat	saturated
o	initial condition

REFERENCES

1. E. A. Ticianelli, C. R. Derouin, A. Redondo, and S. Srinivasan, *This Journal*, **135,** 2209 (1988).
2. S. Srinivasan, S. Somasundaram, D. H. Swan, H. Koch, D. J. Manko, M. A. Enayetulah, and A. J. Appleby, in *Fuel Cells,* R. E. White and A. J. Appleby, Editors, PV 89-14, p. 71, The Electrochemical Society Softbound Proceedings Series, Pennington, NJ 08560 (1989).
3. E. A. Ticianelli, C. R. Derouin, and S. Srinivasan, *J. Electroanal. Chem.*, **251,** 275 (1988).
4. G. A. Eisman in *Fuel Cell Technology and Applications,* PED Management Office for Energy Research, p. 287, The Netherlands (1987).
5. T. F. Fuller and J. Newman, Abstract 87, p. 138, The Electrochemical Society Extended Abstracts, Vol. 92-2, Toronto, ON, Canada Meeting, Oct. 11-16, 1992.
6. T. Nguyen, J. Hedstrom, and N. Vanderborgh, in *Fuel Cells,* R. E. White and A. J. Appleby, Editors, PV 89-14, p. 39, The Electrochemical Society Softbound Proceedings Series, Pennington, NJ (1989).
7. S. Srinivasan and O. Velev, Private communication, 1991.
8. O. J. Murphy, G. D. Hitchens, and D. J. Manko, Abstract 102, p. 158, The Electrochemical Society Extended Abstracts, Vol. 92-2, p. 158, Toronto, ON, Canada Meeting, Oct. 11-16, 1992.
9. P. C. Rieke and N. E. Vanderborgh, *J. Membrane Sci.,* **32,** 313 (1987).
10. T. E. Springer, T. A. Zawodzinski, Jr., and S. Gottesfeld, in *Modeling of Batteries and Fuel Cells,* R. E. White, M. W. Verbrugge, and J. F. Stockel, Editors, PV 91-10, p. 209, The Electrochemical Society Softbound Proceedings Series, Pennington, NJ (1991).
11. P. J. Schutz, in *Fuel Cells,* R. E. White and A. J. Appleby, Editors, PV 89-14, p. 87, The Electrochemical Society Softbound Proceedings Series, Pennington, NJ (1989).
12. T. Nguyen, N. Vanderborgh, and J. Hedstrom, *ibid.,* p. 39,
13. T. Nguyen, J. Guante, and N. Vanderborgh, Paper presented at Materials Research Society Symposium on Solid State Ionics, Boston, MA, Nov. 28-Dec. 2, 1988.
14. T. Zawodzinski, Jr., M. Neeman, L. Sillerud, and S. Gottesfeld, "Determination of Water Diffusion Coefficients in Perfluorosulfonate Ionomeric Membranes," Proceedings of the Symposium on Fuel Cells, The Electrochemical Society, Inc., Pennington, NJ, November 6-7, 1989.
15. T. A. Zawodzinski, Jr., T. E. Springer, J. Davey, J. Valerio, and S. Gottesfeld, in *Modeling of Batteries and Fuel Cells,* R. E. White, M. W. Verbrugge, and J. F. Stockel, Editors, PV 91-10, p. 187, The Electrochemical Society Softbound Proceedings Series, Pennington, NJ (1991).
16. M. W. Verbrugge and R. F. Hill, in *Fuel Cells,* R. E. White and A. J. Appleby, Editors, PV 89-14, p. 1, The Electrochemical Society Softbound Proceedings Series, Pennington, NJ (1989).
17. M. W. Verbrugge and R. F. Hill, *This Journal,* **137,** 886 (1990).
18. M. W. Verbrugge and R. F. Hill, *ibid.,* **137,** 1131 (1990).
19. J. L. Fales, N. E. Vanderborgh, and P. Stroeve, in *Diaphragms, Separators, and Ion-Exchange Membranes,* J. W. Van Zee, R. E. White, and K. Kinoshita, Editors, PV 86-13, p. 179, The Electrochemical Society Softbound Proceedings Series, Pennington, NJ (1986).
20. T. Fuller and J. Newman, in *Fuel Cells,* R. E. White and A. J. Appleby, Editors, PV 89-14, p. 25, The Electrochemical Society Softbound Proceedings Series, Pennington, NJ (1989).
21. D. M. Bernardi, *ibid.,* p. 510.
22. D. M. Bernardi and M. W. Verbrugge, *AIChE J.,* **37,** 1151 (1991).
23. D. M. Bernardi and M. W. Verbrugge, in *Modeling of Batteries and Fuel Cells,* R. E. White, M. W. Verbrugge, and J. F. Stockel, Editors, PV 91-10, p. 240, The Electrochemical Society Softbound Proceedings Series, Pennington, NJ (1991).
24. R. M. Felder and R. W. Rousseau, *Elementary Principles of Chemical Processes,* John Wiley & Sons, Inc., New York (1978).
25. R. H. Perry and C. H. Chilton, *Chemical Engineers' Handbook,* 5th ed., McGraw-Hill Book Co., New York (1973).